Arabian Journal of Chemistry (2022) **15**, 104325

King Saud University

Arabian Journal of Chemistry

www.ksu.edu.sa
www.sciencedirect.com

ORIGINAL ARTICLE

Design of fluorescence system based on rutin functionalized gold nanoparticles: Sensitive detection of etimicin via a smartphone in the food and human samples

Dan Liu, Yilan Zhao, Jiahui Ji, Xiaohua Liu, Shilan Feng *, Xinyue Chen

School of Pharmacy, Lanzhou University, Lanzhou 730000, PR China

Received 6 August 2022; accepted 2 October 2022
Available online 7 October 2022

KEYWORDS

Green-synthesis;
IFE;
Etimicin;
Smartphone sensing platform

Abstract The abuse and contamination of antibiotics have long been a hot issue of global concern. On the basis of inner filter effect (IFE), this article established the fluorescence detection system of a mixture of Rutin-AuNPs and 7-hydroxycoumarin, realizing the rapid and sensitive detection of etimicin. The system was also successfully applied to actual samples through a smartphone sensing platform. Due to the antioxidant property of rutin, Rutin-AuNPs were green synthesized with uniform particle size, good monodispersity, and favorable stability. As a good fluorescent quencher, Rutin-AuNPs could effectively quench the fluorescence of 7-hydroxycoumarin based on IFE with a quenching percent of 89.81 %. However, etimicin could bind tightly to the surface of Rutin-AuNPs through charge attraction, Au-N bond, and affinity between sugars, leading to the replacement of 7-hydroxycoumarin. In addition, one or more of the above effects caused aggregation of Rutin-AuNPs, leading to fluorescence recovery rapidly. A linear response between the fluorescence system and etimicin was reasonably established with detection limits as low as 0.12 μM. This system was successfully applied to real sample detection. Moreover, the great potential smartphone sensing platform was also built for practical application owing to its advantages of digitalization and portability.

* Corresponding author at: Lan Zhou University, School of Pharmacy LANZHOU, Gansu, PR China.
E-mail addresses: Liudan_cpu@163.com (D. Liu), zhaoyl2020@lzu.edu.cn (Y. Zhao), 13606442199@163.com (J. Ji), liuxiaoh@lzu.edu.cn (X. Liu), fengshl@lzu.edu.cn (S. Feng), chenxinyue888@126.com (X. Chen).
Peer review under responsibility of King Saud University.

Production and hosting by Elsevier

https://doi.org/10.1016/j.arabjc.2022.104325
1878-5352

1. Introduction

Etimicin, a semi-synthetic water-soluble aminoglycoside antibiotic, has good effects on the upper respiratory tract, urinary tract, skin, and tissue infection caused by the gram, which can also strengthen the advantages of other aminoglycoside antibiotics (Li et al., 2020; Li et al., 2017; Hayasaki and Sato, 2014). Though etimicin appears to work well in combination or alone, it is also associated with many side effects such as nephrotoxicity, ototoxicity, hepatotoxicity, polymorphic erythema, anaphylaxis, and hyperthermia. Especially for ototoxicity and nephrotoxicity, these adverse reactions would be greatly enhanced by the combination of drugs which should not be ignored. Under the guidelines for rational use of drugs, it is necessary and urgent to monitor the occurrence of adverse drug reactions (Zhuang and Zhang, 2010; Shao et al., 2021). As the side effects of etimicin are closely related to dosage, it is of great importance to developing efficient analytical methods. However, there were few methods for etimicin determination and most of them were high-performance liquid chromatography (HPLC). Despite those instrumental methods having the advantages of sensitivity and accuracy, they suffer from the drawbacks of high cost, complex pre-treatment, and failure to realize real-time online detection due to the particularity of large instruments (Cui et al., 2014; Yuan et al., 2012; Li et al., 2014; Xi et al., 2006; Yao et al., 2017; Wang et al., 2010). It is therefore essential to develop a fast, simple strategy with high sensitivity that also has the advantages of convenience and portability.

The fluorescence-based methods have been broadly used in analytical and bioanalytical applications due to their high sensitivity, convenient signal transduction, simple operation, rapid response, and easy application (Chen et al., 2020; Elahi et al., 2019; Kaur et al., 2019; Min et al., 2022; Yin et al., 2022; Wang et al., 2019; Wang et al., 2022). Mehdi Rahimi et al. constructed a potassium ion optode based on carbon quantum dot fluorescence quenching (Rahimi et al., 2019). Mohamad Mahani1 et al. designed a novel oligosensor was designed using Si quantum dots (SiQDs) for the detection of miRNAs (Mahani et al., 2022). Mohamad Mahani1 et al. designed and fabricated an annexin V-based probe for real-time fluorescence imaging of apoptotic cells using carbon quantum dots as highly stable and biocompatible fluorescent crystals (Mahani et al., 2022). The mechanisms for fluorescence quenching are mainly Förster resonance energy transfer (FRET) and inner filter effect (IFE) (Shen et al., 2022). In general, FRET requires a spectral overlap between the emission of the fluorescent donor and the absorption of the quencher and a distance between the fluorescent donor and the quencher in the range of 1–10 nm. In addition, the donor-quencher distance at FRET efficiency $\eta = 50\ \%$ is referred to as the Förster distance R_0, which is positively correlated with the fluorescence quantum yield of the donor (φ), the dipole orientation factor of the donor and quencher (k), the refractive index of the test medium (n), and the spectral overlap integral of donor emission and quencher absorption (J). In contrast, IFE describes the absorption spectrum of the quencher/acceptor overlapping with the emission and/or excitation spectrum of the fluorescent donor. IFE only needs to satisfy the overlap of the emission spectra of the fluorescent donor and the quencher (Xiong et al., 2022; Sajwan and Solanki, 2022; Wang et al., 2018; Sajwan et al., 2021; Pezhhan et al., 2020). It more effectively converts the absorbance response into a fluorescence intensity change, thus helping to improve the detection sensitivity simply. As the excitation wavelength increases, the donor molecule is excited and enters a higher energy state, and after some time, when it returns to a lower energy (ground) state, additional energy is emitted in the form of photons. The light emitted by the donor is then absorbed by the quencher/acceptor molecule and reduces the fluorescence intensity of the donor molecule. To design an IFE-based fluorescence detection system, a fluorescent donor and a quencher are required. Gold nanoparticles (AuNPs) refer to gold particles with particle sizes ranging from 1 to 100 nm (Cerf and Vieu, 2009). Owing to the special property of Localized Surface Plasmon Resonance (LSPR), AuNPs exhibited unique optical characteristics widely used in the analytical application. LSPR is an attractive optical characteristic of some metal nanoparticles that arises from the resonance of the collective oscillation of the conduction electrons in the noble metal nanoparticles such as gold and silver with the incident photon frequency (Jia et al., 2018; Salahvarzi et al., 2017; Mahani et al., 2021; Mahani et al., 2021; Kim et al., 2018). In view of the high extinction coefficient and strong LSPR absorption centered at 528 nm, the AuNPs are reasonably considered to be a good quencher instead of traditional organic dyes in fluorescence detection (Li et al., 2016). This makes it possible to quench fluorescence by the principle of internal filtration effect (IFE).

As far as known, many physical and chemical methods can be used to prepare AuNPs (Khalaf et al., 2021; Trotsiuk et al., 2020). Generally, the physical method is to directly convert massive metal gold into nano gold according to various dispersion technologies (Hameed, 2021). The chemical method is to chemically reduce chloroauric acid into gold atoms, which would further aggregate to form AuNPs (JyothiKumar et al., 2019). For environmental safety and human health, many green synthesis methods have also attracted great attention (Singh et al. (2021), Kumari and Meena (2020), Sarkar et al. (2021), Susan Punnoose et al., 2021; Wahid et al., 2022). These methods make full use of proteins, plants, microorganisms, and bacteria, in which natural products were most widely used (Kunoh et al., 2017; Kumari and Meena, 2020; Brumbaugh et al., 2014; Dong et al., 2017). Plants are rich in natural active ingredients such as flavonoids, alkaloids, volatile oils, terpenoids, and sugars (Fouda et al., 2020; Wang et al., 2014; Zha et al., 2017). Thus, they can not only act as reducing agents and stabilizers during the synthesis of AuNPs but also act as a modifier to functionalize the surface of AuNPs (Odeniyi et al., 2020; Amjadi et al., 2021). Rutin (Rutin), is a natural flavonoid glycoside, which belongs to flavonol glycosomes widely existing in plants. It widely exists in plants and has the effects of anti-inflammatory, antioxidation, anti-allergy, and anti-virus, especially antioxidant properties (Lins et al., 2021; Semwal et al., 2021; Vimalraj et al., 2021; En-Nakra et al., 2021; Pechyen et al., 2021). It has strong reducibility owing to the abundant hydroxyl groups in the chemical structure. Though many natural products such as green tea, fruit peel, and kaempferia parviflora rhizome extract have been used for the green synthesis of AuNPs (Prema et al., 2022; Anwar et al., 2021; Jiang et al., 2022), their crude extract has the disadvantages of complexity and diversity in ingredients. This may be the main problem existing in a green synthesis that the complex components in crude extract hinder the exploration of the reaction mechanism. For the above reason, the flavonoid monomer compound of rutin was considered, which greatly facilitated the exploration of mechanisms both in green synthesis and testing.

In this study, Rutin-AuNPs were green synthesized with an average size of about 19 nm and a characteristic absorption peak of 528 nm. It was found that when excited at 340 nm, the emission spectrum of 7-hydroxycoumarin at 458 nm overlapped with a large part of the absorption spectrum of Rutin- AuNPs at 528 nm. Thus, 7-hydroxycoumarin could be well quenched by Rutin-AuNPs based on IFE. However, etimicin would strongly interact with Rutin-AuNPs, resulting in the recovery of fluorescence. Therefore, the presumed mechanism of action between Rutin-AuNPs and etimicin was as follows: 1) Rutin contains four phenolic hydroxyl groups, which are acidic and partially negatively charged (Vagish et al. (2021), Martinez and Iverson (2012), Li et al. (2022), Vimalraj et al., 2021; Li et al., 2010), so Rutin-AuNPs synthesized from rutin are also acidic. Etimicin contains amino groups (Xi et al., 2006), which are basic and positively charged. The two interacted by electrostatic force. 2) There were also sites on the surface of Rutin-AuNPs that were not bound by 7-hydroxycoumarin and etimicin was bound to the surface of Rutin-AuNPs via Ag-N bonds (Chen et al., 2022). 3) Rutin is a flavonoid glycoside (Wang et al., 2014), whereas etimicin belongs to the aminogly-

coside class (Yang et al., 2019). There might be an affinity between the two similar to that between sugars. One or more of the above mechanisms acted together, resulting in massive clustering of Rutin-AuNPs, with 7-hydroxycoumarin being competitively replaced. Etimicin was bound to the surface of Rutin-AuNPs. The established system was also successfully applied for real sample detection. Furthermore, it was worth noting that the smartphone sensing platform has been favored in a variety of inspection areas owing to its portability and practicality (Yang et al., 2021; Yuan et al., 2021). The relevant image software on the smartphone allows the conversion of color information into data information that greatly facilitates the quantification of colorimetric detection (Xu et al., 2016). This article established the smartphone sensing platform to realize real sample detection. The color recognizer acquired images taken under a 365 nm UV lamp and converted image information into digital information, building a linear relationship between target and data. Such a smartphone platform emerging in recent years has great potential in the analysis and testing field.

2. Experimental

2.1. Materials

$HAuCl_4{\cdot}3H_2O$ was purchased from Sigma Aldrich Trading Co., ltd (Shanghai, China). 7-Hydroxycoumarin was purchased from Macklin Biochemical Co., ltd (Shanghai, China). Etimicin was purchased from Gaojiaoyan Technology Co., ltd (Beijing, China). Rutin was purchased from Yuanye Biotechnology Co., ltd (Shanghai, China). All the experimental solutions were prepared with ultrapure water.

2.2. Stability study

100 μL, 10 % chloroauric acid solution was dissolved in 20 ml water. It was stirred and heated to 70 ℃. 0.002 g of rutin was dissolved in 5 ml of water and added to the chloroauric acid solution with rapid stirring at once. During the reaction, the color of the solution gradually changed from light yellow to purplish red. The whole reaction was stirred and heated for 10 min. The particle size of Rutin-AuNPs was about 15 nm and the characteristic absorption wavelength was 528 nm. The molar concentration of Rutin-AuNPs was measured to be 1.15 nM by UV–visible spectroscopy using the molar extinction coefficients at the wavelength of the maximum absorption of gold colloid as reported previously [$\varepsilon_{15\ (528nm)} = 3.6 \times 10^8\ cm^{-1}\ M^{-1}$] (Xu et al., 2016).

The effects of different external environments on the stability of Rutin-AuNPs were studied. The effect of pH from 1 to 14 was investigated. The pH of the solution was adjusted with 0.5 M NaOH and 0.5 M HCl. The effect of 20 °C to 90 °C on Rutin-AuNPs was investigated. The effects of 10, 20, 30, 40, and 50 min on the stability of Rutin-AuNPs were determined. The color change of Rutin AuNPs solution was observed and the UV absorption spectrum was monitored.

2.3. The quenching mechanism of 7-Hydroxycoumarin by Rutin-AuNPs

In this section, the optimum concentration and mechanism of Rutin-AuNPs quenching 7-hydroxycoumarin were studied. 0,100, 200, 300, 400, 450,500, 600 μL Rutin-AuNPs were Added to 30 μL 7-hydroxycoumarin solution. The fluorescence color change and fluorescence spectrum were recorded.

2.4. Stability of Rutin-AuNPs and 7-Hydroxycoumarin mixture

The pH of the mixture of Rutin-AuNPs and 7-hydroxycoumarin was adjusted from 1 to 14 with 0.5 M NaOH and 0.5 M HCl to study the effect of environmental changes on fluorescence stability. Changes in fluorescence of Rutin-AuNPs and 7-Hydroxycoumarin mixture in the range of 20 °C to 90 °C were examined to investigate the effect. The effect of time was examined by detecting the fluorescence intensity at 10, 20, 30, 40, 50, and 60 min. Then, Rutin-AuNPs and 7-Hydroxycoumarin mixture with different salt concentrations (increasing from 50 nM to 200 nM) were prepared for the assay. The effect of the external environment on the fluorescence stability was analyzed by UV lamp and fluorescence emission spectrum.

2.5. Fluorescence detection for etimicin

Etimicin at concentrations of 0.20 nM, 0.41 nM, 0.61 nM, 0.82 nM and 1.02 nM was mixed with 480 μL Rutin-AuNPs and 7-Hydroxycoumarin mixture. The fluorescence spectra were measured at an excitation wavelength of 340 nm and an emission wavelength of 458 nm. F and F_0 were the fluorescence intensities in the presence and absence of etimicin, respectively. A calibration curve for the fluorescence recovery rate was established and monitored by $[(F - F_0)/F_0]$.

2.6. Selectivity

Added 10 μL sample to 480 μL Rutin-AuNPs and 7-hydroxycoumarin mixture, ensuring the final concentration was 7.34 nM for all tested substances. The detection method was the same as above.

2.7. Real samples detection via fluorospectrophotometer and smartphones

Human urines, pears, and tomatoes samples were pretreated depending on the usual procedure with minor modifications. Briefly, samples were centrifuged for 10 min at 14,000 rpm. The supernatant was filtered through a 0.22 μm membrane. Urine samples, serum samples, tomato samples, and pear samples were diluted 20 times, 20 times, 30 times, and 20 times respectively. Then a concentration of etimicin was added to each of the treated substrate samples. The whole pretreatment procedure was very simple more than ten minutes. The four samples were treated in the same way. Real samples of a certain concentration of etimicin were prepared and tested.

The smartphone was used as a portable analytical instrument for the on-site testing of etimicin. It was used to analyze the real samples by image capture and color output function. The images of the samples were captured by the smartphone camera under UV light. The color of the image was analyzed by the color analyzer software on the phone. And the color of the images was converted into data (RGB values). A calibration curve of R + G + B versus the concentration of etimicin in the real sample was established.

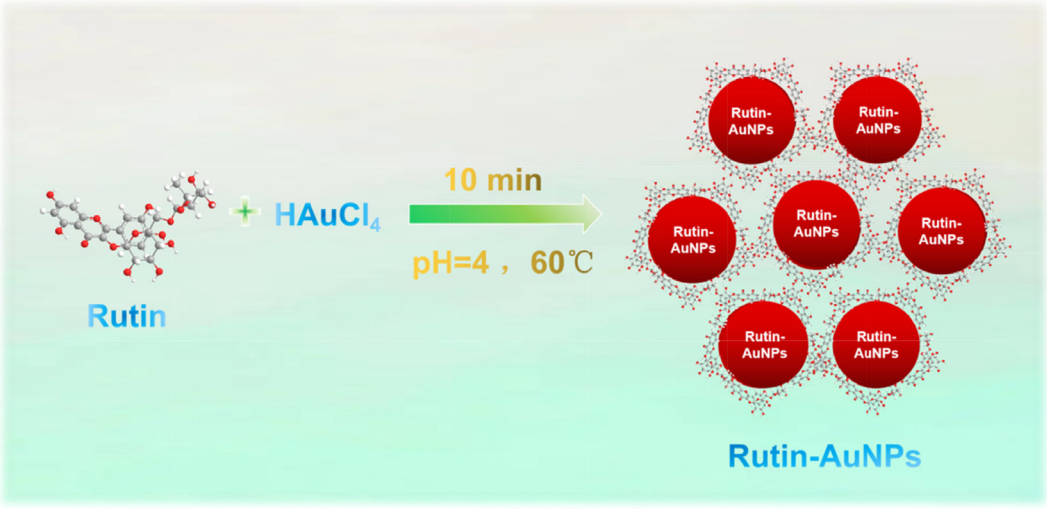

Scheme 1 Green-synthesized Rutin-AuNPs.

3. Results and discussion

3.1. Synthesis of Rutin-AuNPs

Scheme.1 showed the green synthesis of Rutin-AuNPs. Rutin has strong reducing properties which belongs to flavonoid glycosides with abundant hydroxyl. Therefore, in the presence of rutin, free $AuCl_4^-$ in the solution can be reduced to Au (0), which was aggregated to form AuNP. The synthesized Rutin-AuNPs solution showed a purple color. When monitored under a UV–vis spectrophotometer, a characteristic absorption peak was observed at 528 nm with an asymmetrical and narrow shape (Fig. S1A). These results preliminarily indicated that Rutin-AuNPs were well-formed with good dispersion. FT-IR spectra confirmed that the absorption peaks of –OH, -C═O, -C═C and -C─H appeared at 3397.8 cm^{-1}, 1711.0 cm^{-1}, 1617.3 cm^{-1} and 1053.4 cm^{-1} respectively (Fig. S1B). This confirmed that rutin was successfully functionalized on the surface of AuNPs. In conclusion, rutin played an important role in the green synthesis as a reducing agent, stabilizer and modifier. Subsequently, Rutin-AuNPs were extensively characterized and their stability under external environment was investigated. The green synthesized Rutin-AuNPs have uniform dispersion, homogeneous particle size, and good stability.

3.2. Characterization of Rutin-AuNPs

From SEM and TEM images, it was observed that most Rutin-AuNPs were well dispersed in solution with spherical or nearly spherical particle size at about 15 nm (Fig. S1C and Fig. S1D). XPS and EDS results illustrated the element distribution on the surface of Rutin-AuNPs (Fig. S1E and Fig. S2). As shown, the Au ($4f_{7/2}$) and Au ($4f_{5/2}$) binding energies (BE) of the Rutin-AuNPs were detected at 81.3 eV and 85.0 eV, indicating the coexistence of Au (0) and Au^+ in the colloidal Rutin-AuNPs solution (Fig. S2A). Meanwhile, C (1 s) and O(1 s) binding energies were detected at 283.0 eV and 529.5 eV (Fig. S2B and Fig. S2C). EDX also confirmed the presence of C, O, and Au atoms which were mainly derived from rutin (Fig. S1E). Combined with the above FT-IR spectra, these characterization results confirmed that Rutin-AuNPs were functionalized by rutin. The DLS and ZETA result showed that the particle size was about 18.6 ± 1.17 nm with a zeta potential of approximately –22.0 mV, which were consistent with the electron microscope testing results (Fig. S3). And the PDI of Rutin-AuNPs was measured to be 0.276.

3.3. Stability of Rutin-AuNPs

Rutin-AuNPs have uniform particle size and good dispersion at room temperature, accompanied by a characteristic absorption peak at 528 nm. As the external condition plays an important role in the properties of nanoparticles, the stability of Rutin-AuNPs was further studied under various conditions by adjusting pH value, standing time, and temperature. As shown in Fig. S4, the color of the Rutin-AuNPs solution hardly changed as well as the characteristic absorption peak when the pH value was changed from 3 to 14, illustrating that the Rutin-AuNPs could remain stable in acid and alkaline conditions. Only under extreme conditions (pH1-2) were Rutin-AuNPs unable to maintain stable dispersion. It was examined whether the reaction time (10 min − 50 min) would affect the state of Rutin-AuNPs in the solution. The results showed that the Rutin-AuNPs could maintain a stable dispersion state for a certain period (Fig. S5A and Fig. S5B). The effect of temperature on the stability of Rutin-AuNPs was further investigated (Fig. S5C and Fig. S5D). The result indicated the favorable stability of Rutin-AuNPs under the temperature ranging from 20℃ to 80℃. When the temperature increased to 90℃, the absorbance value at 528 nm was slightly changed which had almost no influence on the property of Rutin-AuNPs. From the above, it was clear that the Rutin-AuNPs can maintain a stable dispersion no matter how harsh the external environment was.

3.4. Fluorescence quenching mechanism based on IFE

The quenching efficiency of Rutin-AuNPs on 7-hydroxycoumarin based on IFE was discussed. As can be seen in the Fig. 1A, it was found that the emission spectrum of

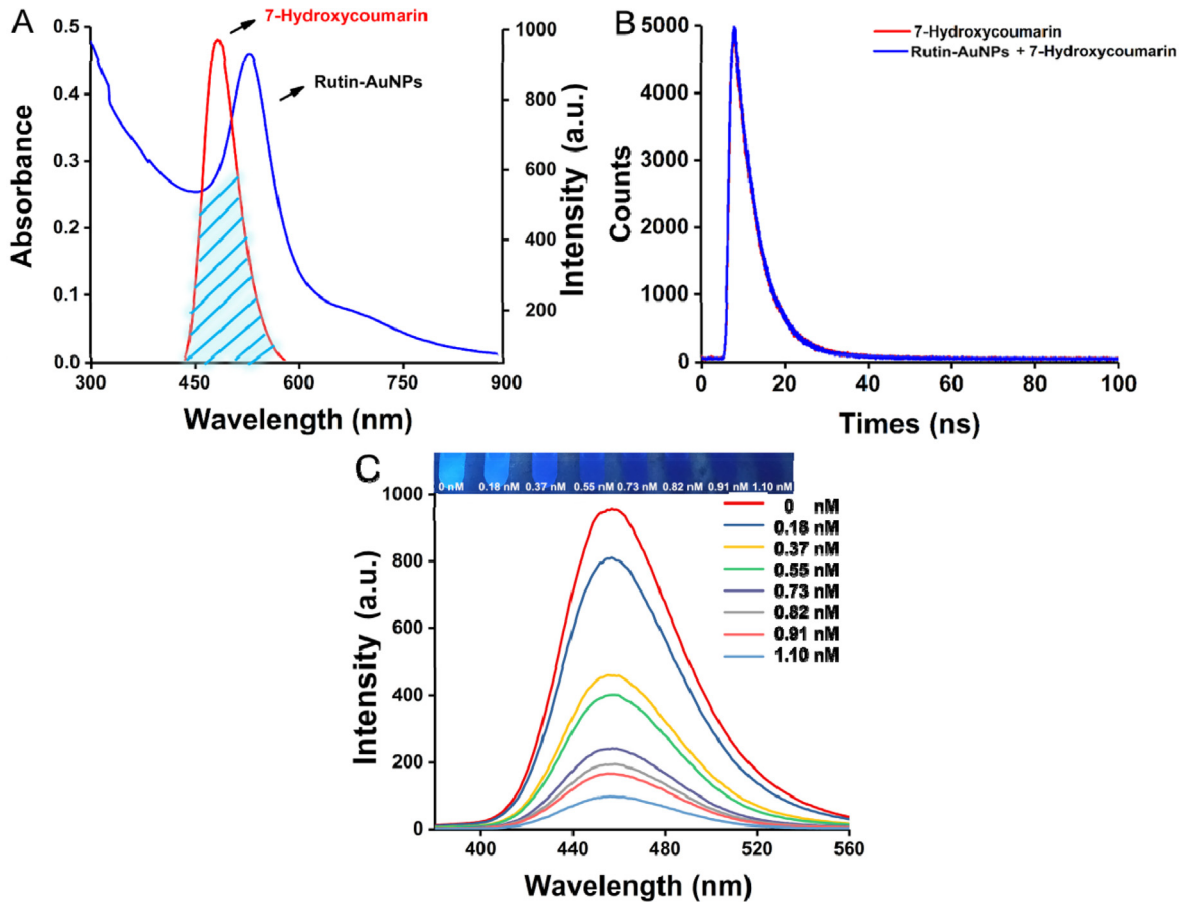

Fig. 1 (A) The absorption spectrum of the Rutin-AuNPs and the fluorescence emission spectrum of 7-Hydroxycumarin. (B) Fluorescence decay traces of 7-Hydroxycumarin and Rutin-AuNPs and 7-Hydroxycumarin mixture. (C) The fluorescence emission spectrum and photograph of 7-Hydroxycumarin with the different concentrations of Rutin-AuNPs.

7-hydroxycoumarin overlapped for the most part with the absorption spectrum of Rutin-AuNPs. The time-resolved fluorescence decay spectra of 7-hydroxycoumarin and the Rutin-AuNPs and 7-Hydroxycoumarin mixture were characterized. As shown in Fig. 1B, the average fluorescence lifetime of 7-hydroxycoumarin and the Rutin-AuNPs and 7-Hydroxycoumarin mixture were calculated to be 5.33 ns and 5.45 ns respectively, suggesting the introduction of Rutin-AuNPs could not change the average fluorescence lifetime of 7-Hydroxycoumarin significantly. Therefore, the IFE resulting from the high overlap of the absorption spectra of Rutin-AuNPs with the emission spectra of 7-hydroxycoumarins may be the main reason for the fluorescence quenching. From the above, Rutin-AuNPs can effectively and rapidly quench the fluorescence of 7-hydroxycoumarin. As can be seen in Fig. 1C, the fluorescence intensity gradually decreased and the fluorescence color gradually darkened as the concentration of Rutin-AuNPs increased from 0.18 nM to 1.10 nM. The results indicated the good quenching performance of Rutin-AuNPs on 7-hydroxycoumarin. After calculation, the quenching percent was 89.81 %. Considering the fluorescence recovery efficiency and system sensitivity, 0.82 nM of Rutin-AuNPs was selected as the optimal concentration of the quenching agent.

3.5. Stability of fluorescence detection system

The stability of the fluorescence detection system of Rutin-AuNPs and the 7-Hydroxycoumarin mixture were investigated (Fig. S6 and Fig. S7). The various conditions were investigated as follows: pH from 1 to 14, temperature from 20 to 90℃, salt concentration from 50 nM to 200 nM, and the mixed solution was kept for 60 min. As the external conditions changed, the fluorescence of 7-hydroxycoumarin remained quenched. Especially for some extremely harsh conditions, there was only a slight change in fluorescence color or spectrum. The results showed that the established fluorescence detection system was stable in various external conditions.

3.6. Detection mechanism of etimicin

As mentioned above, in the absence of etimicin, Rutin-AuNPs rapidly quenched the fluorescence of 7-hydroxycoumarin. However, in the presence of etimicin, the blue fluorescence of 7-hydroxycoumarin was significantly enhanced (Fig. 2). Therefore, the mechanism of action between Rutin-AuNPs and etimicin was postulated to be as follows. 1) Rutin-AuNPs synthesized by rutin were negatively charged. Etimicin was

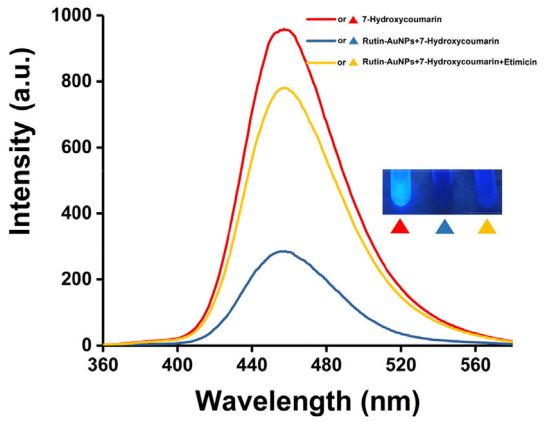

Fig. 2 The fluorescence emission spectrum and photograph of Rutin-AuNPs and 7-Hydroxycumarin mixture in the absence of etimicin and the presence of etimicin.

positively charged. The two interacted by electrostatic force. 2) Etimicin bound to the surface of Rutin-AuNPs through the Ag-N bond. 3) There might be an affinity between rutin and etimicin similar to that between sugars. One or more of the above mechanisms acted together to lead to competitive substitution of 7-hydroxycoumarins and massive aggregation of Rutin-AuNPs (Scheme.2). TEM images of the Rutin-AuNPs and 7-hydroxycoumarin mixture systems in the absence or presence of etimicin were compared to further validate the mechanism (Fig. 3). The results showed that the Rutin-AuNPs and 7-hydroxycoumarin mixture formed massive aggregates in the presence of etimicin. While in the absence of etimicin, the Rutin-AuNPs and 7-hydroxycoumarin mixture were dispersed. The results of the DLS were also compared (Fig. 4). The particle size became much larger after the addition of etimicin which was consistent with the TEM results. The mechanism of fluorescence detection for etimicin was clarified by the above results (Fig. 5).

3.7. Fluorescence determination of etimicin

After a series of optimization for the testing system, the fluorescence detection of etimicin was studied. The results were shown in Fig. S5. 7-Hydroxycoumarin, Rutin-AuNPs, and etimicin coexisted in the solution. Rutin-AuNPs almost completely quenched the fluorescence of 7-hydroxycoumarin accompanied by the absence of etimicin. The fluorescence

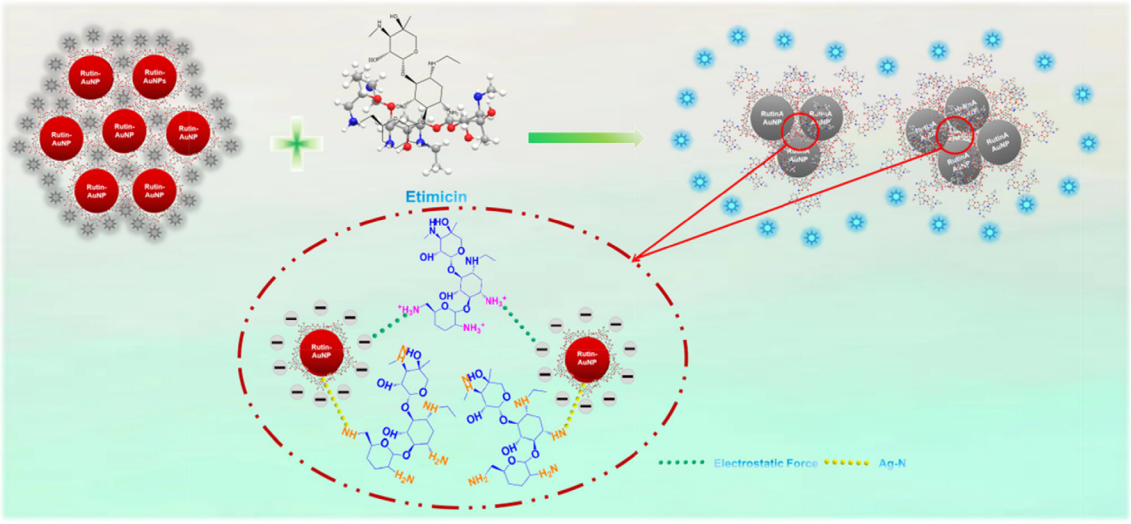

Scheme 2 The mechanism of the IFE-based determination for etimicin.

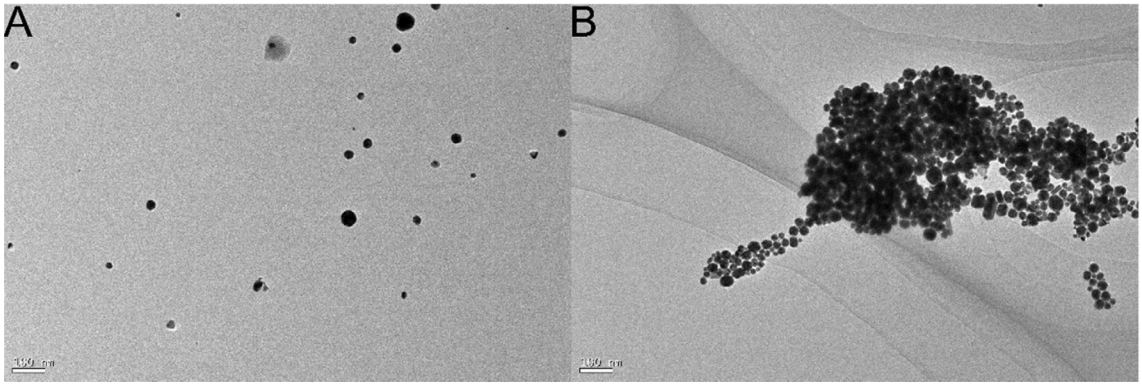

Fig. 3 The TEM image of Rutin-AuNPs and 7-Hydroxycumarin mixture in the absence of etimicin (A) and the presence of etimicin (B).

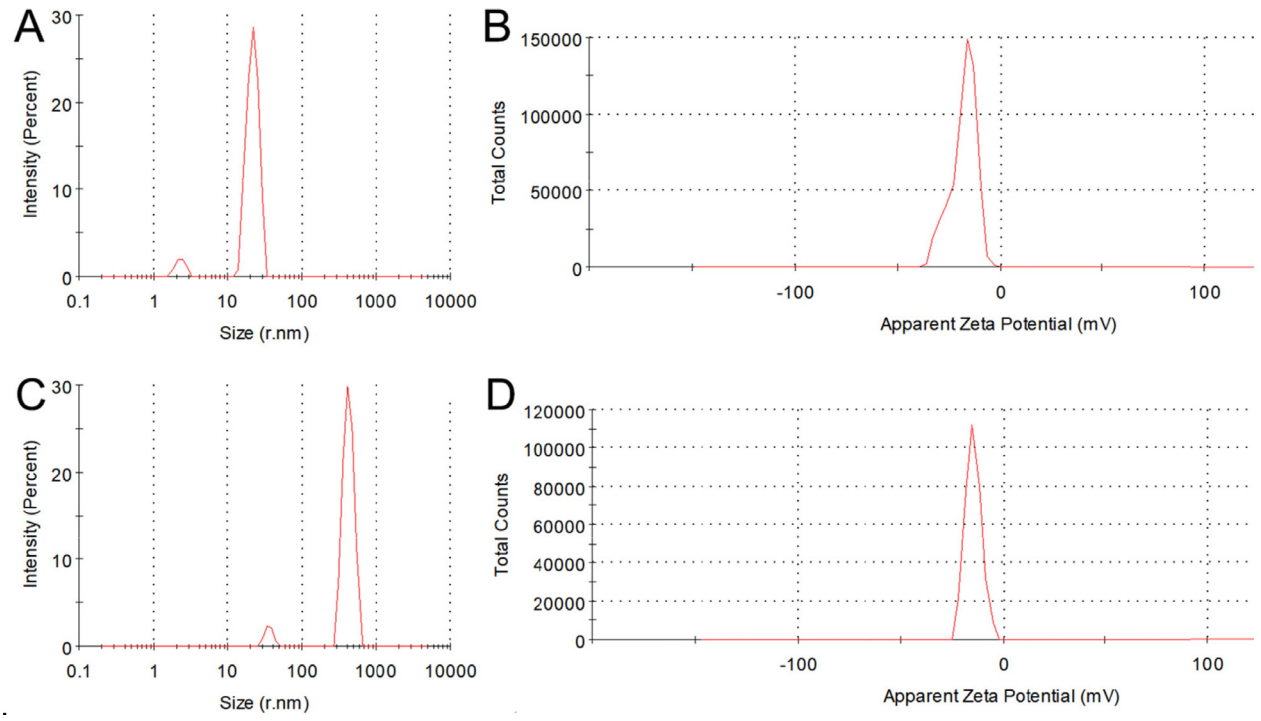

Fig. 4 The particle size distribution of Rutin-AuNPs and 7-Hydroxycumarin mixture in the absence of etimicin (A) and the presence of etimicin (C). The zeta potential of Rutin-AuNPs and 7-Hydroxycumarin mixture in the absence of etimicin (B) and the presence of etimicin (D).

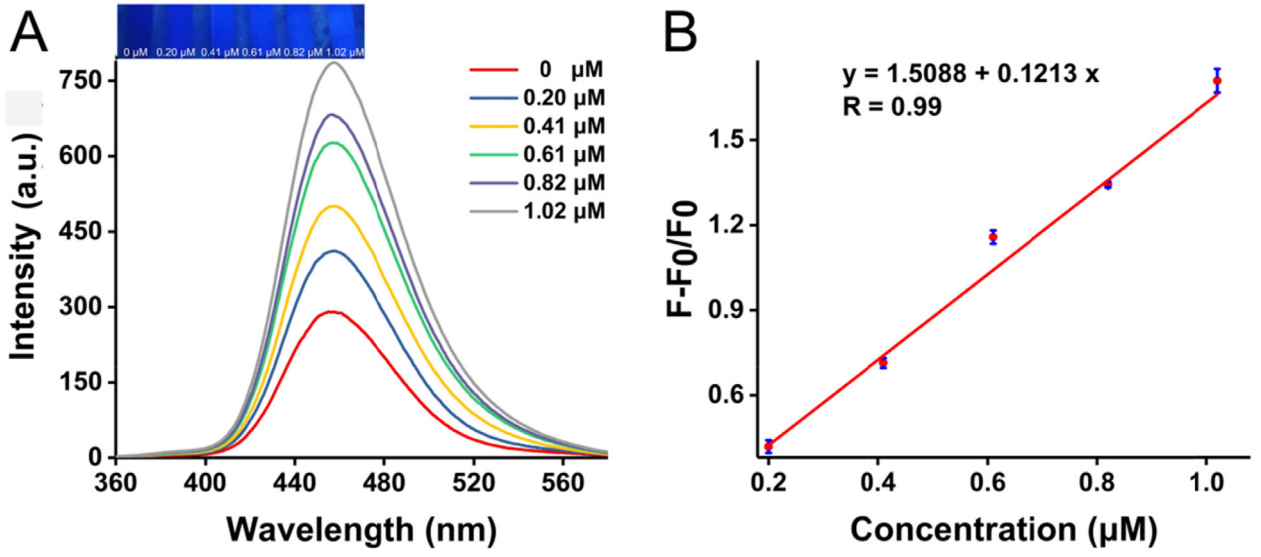

Fig. 5 (A) The fluorescence emission spectrum and photograph of Rutin-AuNPs and 7-Hydroxycumarin mixture in the presence of an increasing concentration of etimicin. (B) The linear calibration of fluorescence recovery efficiency [$(F - F_0)/F_0$] versus the concentration of etimicin.

intensity gradually recovered as the concentration of etimicin increased from 0.20 μM to 1.02 μM, accompanied by the color recovered from black to blue. Under the same conditions, a calibration curve was established between the fluorescence intensity and the concentration of etimicin: $F - F_0/F_0 = 0.04\,90 + 1.6299x$, in which fluorescence intensity in the presence and absence of etimicin was recorded as F and F_0, respectively. The test system LOD was 0.12 μM and the correlation coefficient was 0.99. (LOD = 3 σ/s, where σ represents the standard deviation of the blank and s represents the slope of the linear regression equation.) Table 1 demonstrated the current detection methods for etimicin based on linear range and LOD,

Table 1 Comparison of different detection methods of etimicin.

Various detection methods	Linear range	LOD	Ref.
LC–tandem mass spectrometry	1.04×10^{6}-2.09×10^{8} μM	1.04×10^{-4} μM	(Cui et al., 2014)
Silver nanoparticles for visual colorimetric detection	0.33–0.68 μM	0.36 μM	(Li et al., 2014)
Liquid chromatography	10.46–2.62×10^{3} μM	-	(Xi et al., 2006)
LC-MS/MS method	0.1–4.19 μM	-	(Yao et al., 2017)
Resonance Rayleigh-scattering spectral method	0.04–12.56 μM	9.42×10^{-3} μM	(Wang et al., 2010)
This work	0.20–1.02 μM	0.12 μM	–

indicating that our testing system had low LOD in a relatively wide range. Besides, most of the reported methods suffer from the drawbacks of expensive equipment and complex pre-processing to some extent limiting the application of the laboratory. Thus, this article established a sensitive, rapid and visual fluorescence method, which was expected to apply in real sample detection.

3.8. Selectivity study

To further investigate the selectivity of the fluorescence testing system towards etimicin, common interfering substances such as thiamphenico, roxithromycin, clarithromycin, erythromycin, penicillin potassium, ampicillin, amoxicillin, sulfadiazine, clindamycin, ofloxacin, tetracycline, trimethoprim were compared (Fig. 6). The final concentration of all substances was 4.09 μM. When etimicin was added to Rutin-AuNPs and 7-hydroxycoumarin mixture, the fluorescence intensity of the solution was significantly enhanced with the blue fluorescence observed under a UV lamp. Whereas the quenched fluorescence could not be restored when Rutin-AuNPs and 7-hydroxycoumarin coexisted with other antibiotics, respectively. The result of color change was always consistent with that of the fluorescence spectrum. From the above, the testing system showed great selectivity towards etimicin, ensuring its use in practical applications. To sum up the above, the previous discussion of the mechanism and the preliminary experiments showed that the superior selectivity of etimicin in this analytical system was mainly due to its superior structure. Etimicin belongs to the aminoglycosides class, and its close binding to Rutin-AuNPs through a unique structure restored the fluorescence of 7-hydroxycoumarin, which ultimately enabled fluorescence detection. It can be seen that the detection system has a strong response value for all aminoglycosides.

3.9. Application in real samples

To comprehensively investigate the application, various samples including pears, tomatoes, and a biological sample of urines and serums were prepared (Fig. 7). After simple pretreatment, a series of concentrations of etimicin were spiked into the prepared samples. The experimental operation was as described above. As the spiked concentrations of serum, urine, pear, and a tomato increased from 2.04 to 12.24 μM, 0.41 to 6.12 μM, 1.02 to 8.16 μM, and 0.41 to 4.08 μM respectively, the blue fluorescence of 7-hydroxycoumarin gradually recovered in all four samples, with a significant increase in fluorescence intensity at 458 nm. The linear ranges, linear equations, and correlation coefficients for the actual samples

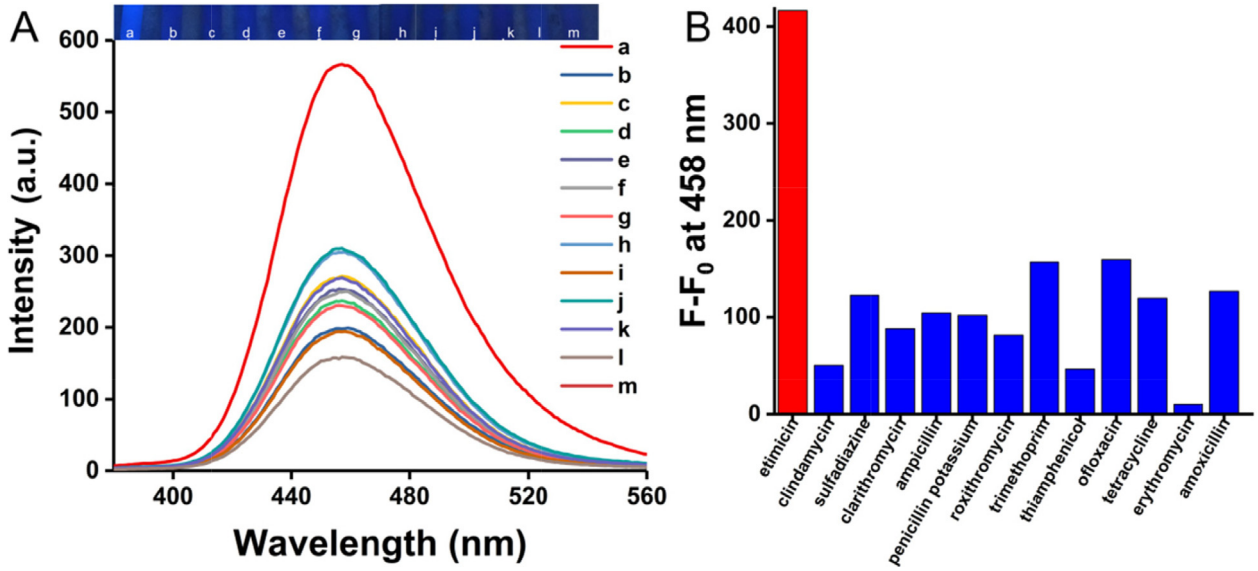

Fig. 6 (A) The fluorescence emission and photograph of the selectivity of Rutin-AuNPs and 7-Hydroxycumarin mixture (from a to m: etimicin, clindamycin, sulfadiazine, clarithromycin, ampicillin, penicillin potassium, roxithromycin, trimethoprim, thiamphenicol, ofloxacin, tetracycline, erythromycin, and amoxicillin, all of the concentration are 4.09 μM). (B) The histogram corresponds to (A), F_0 is the fluorescence intensity value of the blank.

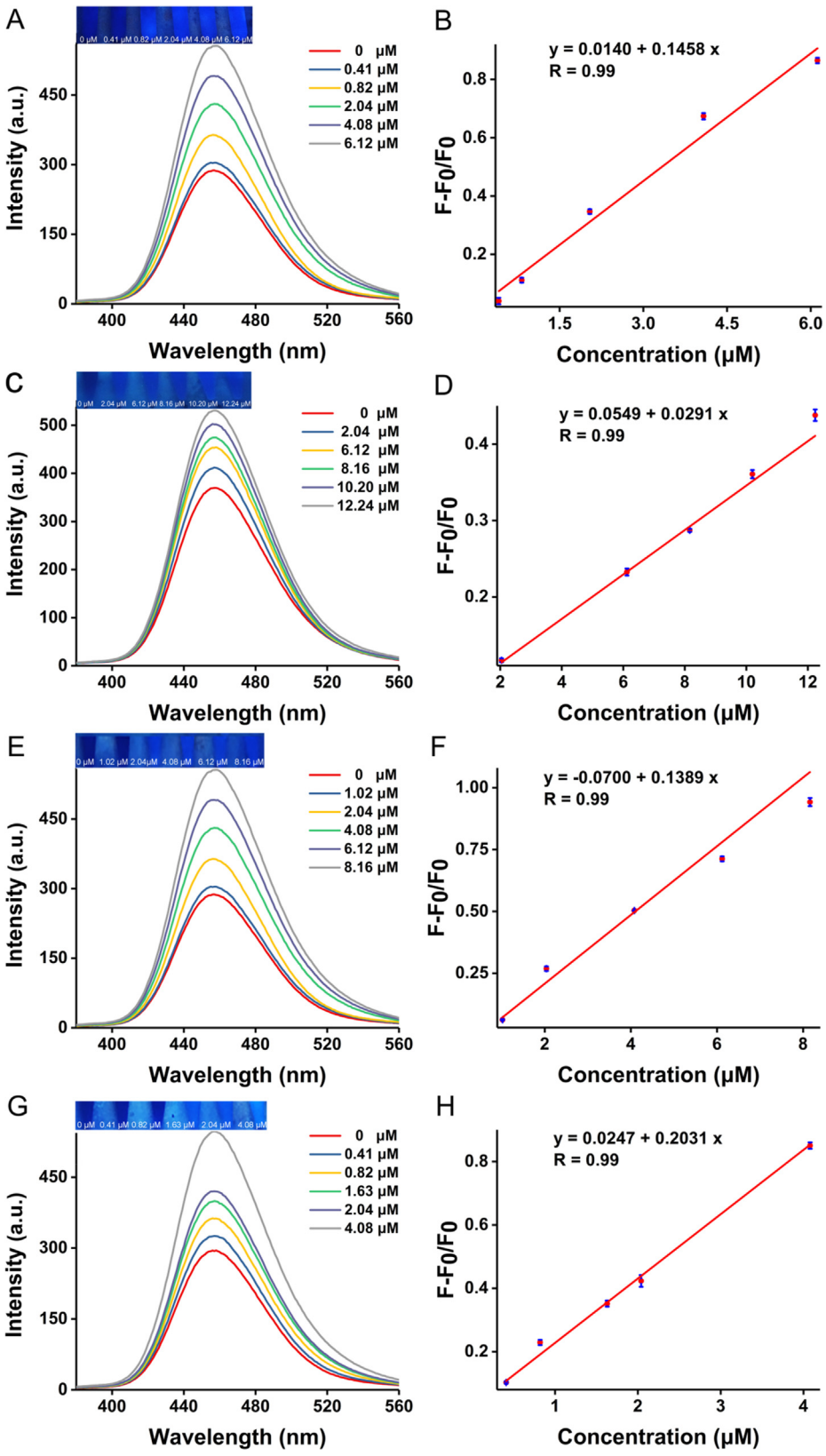

Fig. 7 The fluorescence emission spectrum and photograph of Rutin-AuNPs and 7-Hydroxycumarin mixture in the presence of increasing concentrations of etimicin in serum (A) urine (C), pears (E), and tomatoes (G). The linear calibration of fluorescence recovery efficiency $[(F - F_0)/F_0]$ versus the concentration of etimicin in serum (B), urine (D), pears (F), and tomatoes (H).

Table 2 The linear calibration of fluorescence recovery efficiency [(F - F_0)/F_0] versus the concentration of etimicin in the real sample.

Real Samples	Linear curve	Linear range	R
Urine	F - F_0/F_0 = 0.0140 + 0.1458 x	0.41–6.12 μM	0.99
Serum	F - F_0/F_0 = 0.0549 + 0.0291 x	2.04–12.24 μM	0.99
Pears	F - F_0/F_0 = -0.0700 + 0.1389 x	1.02–8.16 μM	0.99
Tomatoes	F - F_0/F_0 = 0.0247 + 0.2031 x	0.41–4.08 μM	0.99

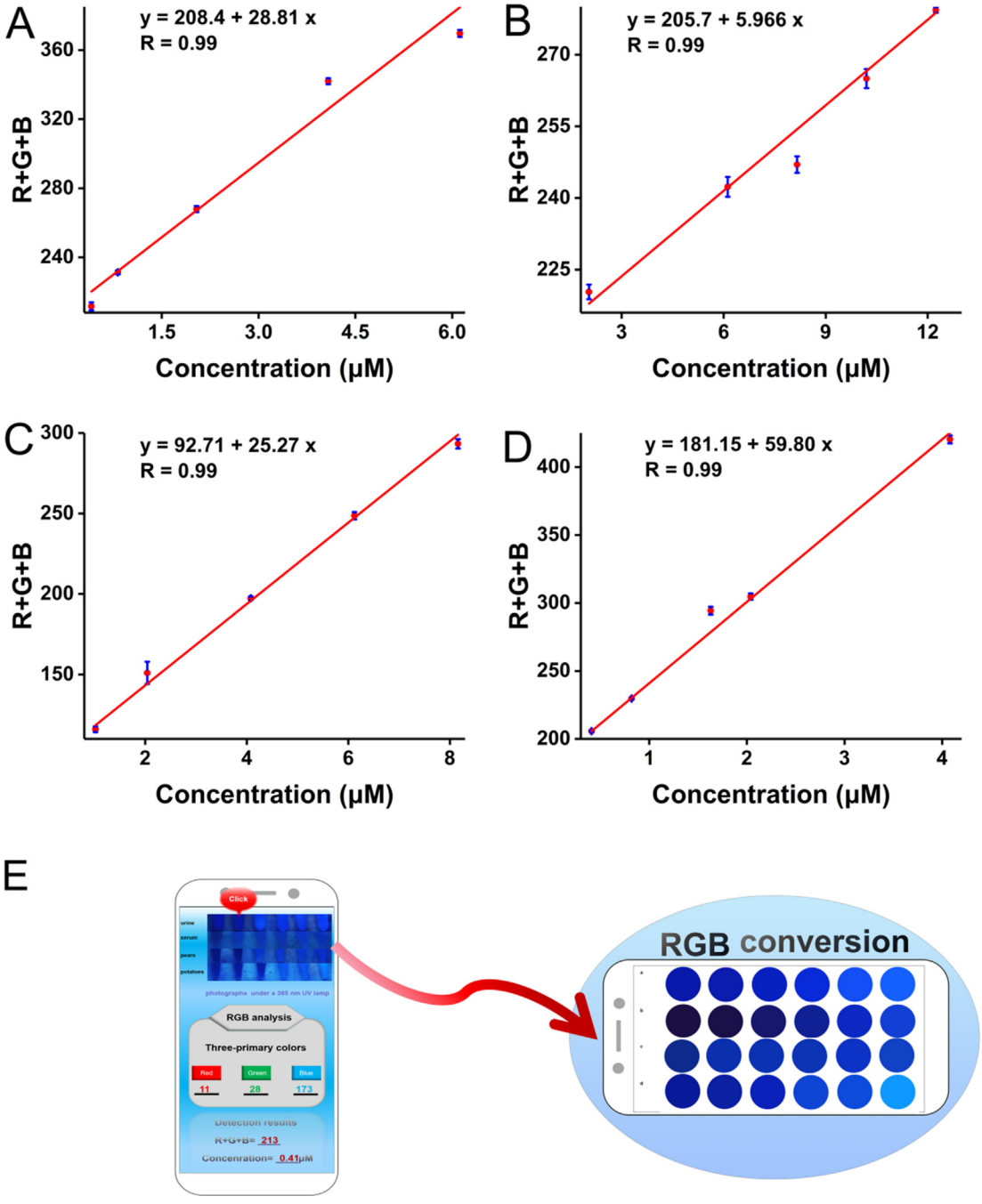

Fig. 8 The linear calibration of values of R + G + B (analyzed by the color recognizer of the smartphone) versus the etimicin concentration in urine (A), serum (B), pears (C), and tomatoes (D). The fluorescence photographs (taken by a 365 nm UV lamp) were processed by a smartphone sensing platform (E).

Table 3 The linear calibration of the values of R + G + B versus the etimicin concentration in the real sample based on a smartphone sensing platform.

Real Samples	Linear curve	Linear range	R
Urine	$F - F_0/F_0 = 208.4 + 28.81\ x$	0.41–6.12 μM	0.99
Serum	$F - F_0/F_0 = 205.7 + 5.966\ x$	2.04–12.24 μM	0.99
Pears	$F - F_0/F_0 = 92.71 + 25.27\ x$	1.02–8.16 μM	0.99
Tomatoes	$F - F_0/F_0 = 181.15 + 59.80\ x$	0.41–4.08 μM	0.99

were shown in Table 2. The results showed that the fluorescence detection system was highly sensitive with correlation coefficients of 0.99 in all cases. The detection system could establish a good linear relationship with all four samples. It was able to quantify different types of actual samples and had good application prospects in actual sample detection. The smartphone sensing platform that emerged in recent years greatly facilitates the quantification of colorimetric detection. In this paper, the smartphone camera acted as a high-performance light detector. The images of the samples were captured by the smartphone camera under 365 nm UV light. The color of the image was analyzed by the color analyzer software on the phone. And the color of the images was converted into data (RGB values). Analysis by the RGB channel was performed by a mobile application app on the smartphone. The app used for RGB analysis was developed by XiYi Technology Co., ltd. in Xiamen, China (named Colour Identifier). The value of R + G + B was used to reflect the concentration of etimicin. A linear relationship between R + G + B and the concentration of the target was established (Fig. 8E). The results showed a good linear relationship between the R + G + B value and the concentration of etimicin spiked in the actual samples (Fig. 8A, Fig. 8B, Fig. 8C, and Fig. 8D). Table 3 showed the linear ranges, linear equations, and correlation coefficients for the actual samples. The results showed that the sensing platform was highly sensitive with good correlation coefficients of 0.99. Thus, the smartphone sensing platform could quantitatively, conveniently, intuitively, and sensitively detect etimicin in real samples.

4. Conclusion

The established fluorescence system based on Rutin-AuNPs had the following advantages: 1) Rutin-AuNPs were green synthesized by a one-pot method with uniform particle size and good stability. 2) The article used the monomer compound of rutin rather than the crude extract of a plant which was beneficial to the in-depth study of the reaction mechanism. 3) The fluorescence of 7-hydroxycoumarin could be effectively quenched by Rutin-AuNPs based on IFE. 4) A strong covalent bonding would occur between Rutin-AuNPs and etimicin, leading to the replacement of 7-hydroxycoumarin and the rapid recovery of fluorescence. 5) The established fluorescence system was successfully applied in real sample detection and a portable smartphone sensing platform was established.

Declaration of Competing Interest

The authors declare that they have no known competing financial interests or personal relationships that could have appeared to influence the work reported in this paper.

Acknowledgments

Natural Science Foundation of Gansu Province, 21JR7RA400; Cuiying Scientific and Technological Innovation Program of Lanzhou University Second Hospital, CY2021-QN-A07).

Appendix A. Supplementary material

Supplementary data to this article can be found online at https://doi.org/10.1016/j.arabjc.2022.104325.

References

Amjadi, S., Shahnaz, F., Shokouhi, B., Azarmi, Y., Siahi-Shadbad, M., Ghanbarzadeh, S., Kouhsoltani, M., Ebrahimi, A., Hamishehkar, H., 2021. Nanophytosomes for enhancement of rutin efficacy in oral administration for diabetes treatment in streptozotocin-induced diabetic rats. Int. J. Pharm. 121208.

Anwar, Y., Ullah, I., Ul-Islam, M., Alghamdi, K.M., Khalil, A., Kamal, T., 2021. Adopting a green method for the synthesis of gold nanoparticles on cotton cloth for antimicrobial and environmental applications. Arabian J. Chem. 14, (9) 103327.

Brumbaugh, A.D., Cohen, K.A., St, S.K., 2014. Angelo, Ultrasmall Copper Nanoparticles Synthesized with a Plant Tea Reducing Agent. ACS Sustainable Chem. Eng. 2 (8), 1933–1939.

Cerf, A., Vieu, C., 2009. Transfer printing of sub-100nm nanoparticles by soft lithography with solvent mediation. Colloids Surf., A 342 (1–3), 136–140.

Chen, H., Hu, O., Fan, Y., Xu, L., Zhang, L., Lan, W., Hu, Y., Xie, X., Ma, L., She, Y., Fu, H., 2020. Fluorescence paper-based sensor for visual detection of carbamate pesticides in food based on CdTe quantum dot and nano ZnTPyP. Food Chem. 327, 127075.

Chen, M., Zhou, H., Huang, C., Liu, P., Fei, J., Ou, J., Ou, S., Zheng, J., 2022. Identification and cytotoxic evaluation of the novel rutin-methylglyoxal adducts with dione structures in vivo and in foods. Food Chem 377, 132008.

Cui, Y., Ma, N., Li, X., Lv, C., Li, M., Li, M., Song, L., Liu, M., Li, Q., Bi, K., 2014. Development of an ultra fast liquid chromatography-tandem mass spectrometry method for simultaneous determination of cefazedone and etimicin in beagle dog plasma: Application to the pharmacokinetic study of the combination of cefazedone and etimicin injections. Journal Chromatography B-analytical technologies in the Biomedical and life sciences 973C, 97–103.

Dong, C., Cao, C., Zhang, X., Zhan, Y., Wang, X., Yang, X., Zhou, K., Xiao, X., Yuan, B., 2017. Wolfberry fruit (Lycium barbarum) extract mediated novel route for the green synthesis of silver nanoparticles. Optik 130, 162–170.

Elahi, N., Kamali, M., Baghersad, M.H., Amini, B., 2019. A fluorescence Nano-biosensors immobilization on Iron (MNPs) and gold (AuNPs) nanoparticles for detection of Shigella spp. Materials Science & Engineering C-Materials for Biological Applications 105, 110113.

En-Nakra, F., Uzun, D., Hasdemir, E., 2021. Voltammetric determination of rutin in fruit juice samples using a 2 mercaptobenzothiazole coated pencil graphite electrode. J. Food Compos. Anal. 104, 104183.
Fouda, M.M.G., Ajarem, J.S., Maodaa, S.N., Allam, A.A., Taher, M. M., Ahmed, M.K., 2020. Carboxymethyl cellulose supported green synthetic features of gold nanoparticles: Antioxidant, cell viability, and antibacterial effectiveness. Synth. Met. 269, 116552.
Hameed, R., 2021. Synthesis and physical properties of nanocomposite gold nanoparticles attached to graphene quantum dots prepared by laser ablation. Mater. Today:. Proc. 42, 1829–1833.
Hayasaki, Y., Sato, A., 2014. Holographic three-dimensional motion detection of an optically trapped sub-100nm gold nanoparticle. Opt. Commun. 322, 22–26.
Jia, S., Bian, C., Sun, J., Tong, J., Xia, S., 2018. A wavelength-modulated localized surface plasmon resonance (LSPR) optical fiber sensor for sensitive detection of mercury(II) ion by gold nanoparticles-DNA conjugates. Biosens. Bioelectron. 114, 15–21.
Jiang, S., Meng, X., Xu, M., Li, M., Li, S., Wang, Q., Liu, W., Hao, L., Wang, J., Wang, C., Wang, Z., Wu, Q., 2022. Green synthesis of novel magnetic porous organic polymer for magnetic solid phase extraction of neonicotinoids in lemon juice and honey samples. Food Chem. 12599.
JyothiKumar, A., Kailasnath, M., Simon, J., Mathew, S., 2019. BSA Stabilized Gold Nanoparticles: Synthesis and Characterization. Mater. Today:. Proc. 9, 111–115.
Kaur, H., Singh, N., Kaur, N., Jang, D.O., 2019. Nano-aggregate-Fe^{3+} complex based on benzimidazole-modified calix[4]arene for amplified fluorescence detection of ADP in aqueous media. Sens. Actuators, B 284, 193–201.
Khalaf, M.M., Abd El-Lateef, H.M., Mohamed, I.M.A., Zaki, M.E. A., Toghan, A., 2021. Facile synthesis of gold-nanoparticles by different capping agents and their anticancer performance against liver cancer cells, Colloid and Interface Science. Communications 44, 100482.
Kim, J., Oh, S.Y., Shukla, S., Hong, S.B., Heo, N.S., Bajpai, V.K., Chun, H.S., Jo, C.H., Choi, B.G., Huh, Y.S., Han, Y.K., 2018. Heteroassembled gold nanoparticles with sandwich-immunoassay LSPR chip format for rapid and sensitive detection of hepatitis B virus surface antigen. HBsAg. Biosens. Bioelectron. 107, 118–122.
Kumari, P., Meena, A., 2020. Green synthesis of gold nanoparticles from Lawsoniainermis and its catalytic activities following the Langmuir-Hinshelwood mechanism. Colloids Surf., A 606, 124447.
Kumari, P., Meena, A., 2020. Green synthesis of gold nanoparticles from Lawsoniainermis and its catalytic activities following the Langmuir-Hinshelwood mechanism. Colloids Surf., A 606, 125447.
Kunoh, T., Takeda, M., Matsumoto, S., Suzuki, I., Takano, M., Kunoh, H., Takada, J., 2017. Green Synthesis of Gold Nanoparticles Coupled with Nucleic Acid Oxidation. ACS Sustainable Chem. Eng. 6 (1), 364–373.
Li, N., Gu, Y., Gao, M., Wang, Z., Xiao, D., Li, Y., Wang, J., He, H., 2014. Label-free silver nanoparticles for visual colorimetric detection of etimicin. Anal. Methods 6 (19), 7906–7911.
Li, L., Li, B., Cheng, D., Mao, L., 2010. Visual detection of melamine in raw milk using gold nanoparticles as colorimetric probe. Food Chem. 122 (3), 895–900.
Li, Y., Peng, Z., Tan, L., Zhu, Y., Zhao, C., Zeng, Q.H., Liu, G., Wang, J.J., Zhao, Y., 2022. Structural and functional properties of soluble Antarctic krill proteins covalently modified by rutin. Food Chem 379, 132159.
Li, J., Xiao, Y., Qin, H., Shi, H., Huang, H., Zhang, Y., He, X., Wang, K., 2017. A bispyrene/AgNP-based ratiometric nanoprobe for supersensitive fluorescence and colorimetric sensing of etimicin. Anal. Methods 9 (25), 3845–3851.
Li, Y., Xu, J., Wang, L., Huang, Y., Guo, J., Cao, X., Shen, F., Luo, Y., Sun, C., 2016. Aptamer-based fluorescent detection of bisphenol A using nonconjugated gold nanoparticles and CdTe quantum dots. Sens. Actuators, B 222, 815–822.
Li, N., Yu, F., Peng, F., Zhang, X., Jia, B., 2020. Probable sexual transmission of brucellosis. IDCases 21, e00871.
Lins, T., Barberino, R.S., Monte, A.P.O., Pinto, J.G.C., Campinho, D. S.P., Palheta Jr., R.C., Matos, M.H.T., 2021. Rutin promotes activation and reduces apoptosis of primordial follicles by regulating Akt phosphorylation after in vitro culture of ovine ovarian tissue. Theriogenology 173, 64–72.
Mahani, M., Alimohamadi, F., Torkzadeh-Mahani, M., Hassani, Z., Khakbaz, F., Divsar, F., Yoosefian, M., 2021. LSPR biosensing for the early-stage prostate cancer detection using hydrogen bonds between PSA and antibody: Molecular dynamic and experimental study. J. Mol. Liq. 324, 114736.
Mahani, M., Taheri, M., Divsar, F., Khakbaz, F., Nomani, A., Ju, H., 2021. Label-free triplex DNA-based biosensing of transcription factor using fluorescence resonance energy transfer between N-doped carbon dot and gold nanoparticle. Anal. Chim. Acta 1181, 338919.
Mahani, M., Karimi-Mazidi, P., Khakbaz, F., Torkzadeh-Mahani, M., 2022. Carbon quantum dots—Annexin V probe: photoinduced electron transfer mechanism, phosphatidylserine detection, and apoptotic cell imaging. Microchim. Acta 189, 69.
Mahani, M., Khakbaz, F., Ju, H., 2022. Hairpin oligosensor using SiQDs: Forster resonance energy transfer study and application for miRNA-21 detection. Anal. Bioanal. Chem. 414, 2505–2512.
Martinez, C.R., Iverson, B.L., 2012. Rethinking the term "pi-stacking". Chem. Sci. 3 (7), 2191–2201.
Min, X., Yi, F., Han, X.-L., Li, M., Gao, Q., Liang, X., Chen, Z., Sun, Y., Liu, Y., 2022. Targeted photodynamic therapy using a water-soluble aggregation-Induced emission photosensitizer activated by an acidic tumor microenvironment. Chem. Eng. J. 432.
Odeniyi, M.A., Okumah, V.C., Adebayo-Tayo, B.C., Odeniyi, O.A., 2020. Green synthesis and cream formulations of silver nanoparticles of Nauclea latifolia (African peach) fruit extracts and evaluation of antimicrobial and antioxidant activities. Sustainable Chem. Pharm. 15, 100197.
Pechyen, C., Ponsanti, K., Tangnorawich, B., Ngernyuang, N., 2021. Waste fruit peel – Mediated green synthesis of biocompatible gold nanoparticles. J. Mater. Res. Technol. 14, 2982–2991.
Pezhhan, H., Akhond, M., Shamsipur, M., 2020. Histidine capped-gold nanoclusters mediated fluorescence detection of glucose and hydrogen peroxide based on glucose oxidase-mimicking property of gold nanoparticles via an inner filter effect mechanism. J. Lumin. 228, 117604.
Prema, P., Boobalan, T., Arun, A., Rameshkumar, K., Suresh Babu, R., Veeramanikandan, V., Nguyen, V.-H., Balaji, P., 2022. Green tea extract mediated biogenic synthesis of gold nanoparticles with potent anti-proliferative effect against PC-3 human prostate cancer cells. Mater. Lett. 306, 130882.
Rahimi, M., Mahani, M., Hassani, Z., 2019. Carbon quantum dots fluorescence quenching for potassium optode construction. Luminescence 34, 402–406.
Sajwan, R.K., Lakshmi, G.B.V.S., Solanki, P.R., 2021. Fluorescence tuning behavior of carbon quantum dots with gold nanoparticles via novel intercalation effect of aldicarb. Food Chem. 340, 127835.
Sajwan, R.K., Solanki, P.R., 2022. A hybrid optical strategy based on graphene quantum dots and gold nanoparticles for selective determination of gentamicin in the milk and egg samples. Food Chem. 370, 131312.
Salahvarzi, A., Mahani, M., Torkzadeh-Mahani, M., Alizadeh, R., 2017. Localized surface plasmon resonance based gold nanobiosensor: Determination of thyroid stimulating hormone. Anal. Biochem. 516, 1–5.
Sarkar, S., Bhowal, A.C., Kandimalla, R., Kundu, S., 2021. Structural and electrical behaviours of PEDOT:PSS thin films in presence of

negatively charged gold and silver nanoparticles: A green synthesis approach. Synth. Met. 279, 116848.
Semwal, R., Joshi, S.K., Semwal, R.B., Semwal, D.K., 2021. Health benefits and limitations of rutin - A natural flavonoid with high nutraceutical value. Phytochem. Lett. 46, 119–128.
Shao, W., Zhong, D., Jiang, H., Han, Y., Yin, Y., Li, R., Qian, X., Chen, D., Jing, L., 2021. A new aminoglycoside etimicin shows low nephrotoxicity and ototoxicity in zebrafish embryos. Journal of applied toxicology: JAT 41 (7), 1063–1075.
Shen, Y., Nie, C., Wei, Y., Zheng, Z., Xu, Z.-L., Xiang, P., 2022. FRET-based innovative assays for precise detection of the residual heavy metals in food and agriculture-related matrices. Coord. Chem. Rev. 469.
Singh, T., Jayaprakash, A., Alsuwaidi, M., Madhavan, A.A., 2021. Green synthesized gold nanoparticles with enhanced photocatalytic activity. Mater. Today:. Proc. 42, 1166–1169.
Susan Punnoose, M., Bijimol, D., Mathew, B., 2021. Microwave assisted green synthesis of gold nanoparticles for catalytic degradation of environmental pollutants. Environ. Nanotechnol. Monit. Manage. 16, 100525.
Trotsiuk, L., Antanovich, A., Lizunova, A., Kulakovich, O., 2020. Direct synthesis of amphiphilic polyvinylpyrrolidone-capped gold nanoparticles in chloroform. Colloid Interface Sci. Commun. 37, 100289.
Vagish, C.B., Kumara, K., Vivek, H.K., Bharath, S., Lokanath, N.K., Ajay Kumar, K., 2021. Coumarin-triazole hybrids: Design, microwave-assisted synthesis, crystal and molecular structure, theoretical and computational studies and screening for their anticancer potentials against PC-3 and DU-145. J. Mol. Struct. 1230, 129899.
Vimalraj, S., Saravanan, S., Subramanian, R., 2021. Rutin-Zn(II) complex promotes bone formation - A concise assessment in human dental pulp stem cells and zebrafish. Chem. Biol. Interact. 349, 109674.
Wahid, I., Rani, P., Kumari, S., Ahmad, R., Hussain, S.J., Alamri, S., Tripathy, N., Khan, M.I.R., 2022. Biosynthesized gold nanoparticles maintained nitrogen metabolism, nitric oxide synthesis, ions balance, and stabilizes the defense systems to improve salt stress tolerance in wheat. Chemosphere 287, 132142.
Wang, X., Chen, Z., Yin, J., Liu, S.H., 2022. Mononuclear aggregation-induced emission (AIE)-active gold(I)-isocyanide phosphors: Contrasting phosphorescent mechanochromisms and effect of halogen substitutions on room-temperature phosphorescence nature. Chin. Chem. Lett. 33, 2522–2526.
Wang, Z., Fang, C., Megharaj, M., 2014. Characterization of Iron-Polyphenol Nanoparticles Synthesized by Three Plant Extracts and Their Fenton Oxidation of Azo Dye. ACS Sustainable Chem. Eng. 2 (4), 1022–1025.
Wang, X.Y., Hu, Y.X., Yang, X.F., Yin, J., Chen, Z., Liu, S.H., 2019. Excitation Wavelength-Dependent Nearly Pure White Light-Emitting Crystals from a Single Gold(I)-Containing Complex. Org Lett 21, 9945–9949.
Wang, L., Peng, J., Liu, Z., He, Y., 2010. Resonance Rayleigh-scattering spectral method for the determination of some aminoglycoside antibiotics using CdTe quantum dots as a probe. Luminescence 25 (6), 424–430.
Wang, M., Wang, L., Liu, Q., Su, X., 2018. A fluorescence sensor for protein kinase activity detection based on gold nanoparticles/copper nanoclusters system. Sens. Actuators, B 256, 691–698.
Wang, Y., Zhang, Z., Wu, L., Zhang, X., Wang, H., Ye, W., Li, P., 2014. Isolation and structure characterization of related impurities in etimicin intermediate P1 by LC/ESI-MS(n) and NMR. J Pharm Biomed Anal 97, 97–102.
Xi, L., Wu, G., Zhu, Y., 2006. Analysis of etimicin sulfate by liquid chromatography with pulsed amperometric detection. J. Chromatogr. A 1115 (1–2), 202–207.
Xiong, J., He, S., Wang, Z., Xu, Y., Zhang, L., Zhang, H., Jiang, H., 2022. Dual-readout fluorescence quenching immunochromatographic test strips for highly sensitive simultaneous detection of chloramphenicol and amantadine based on gold nanoparticle-triggered photoluminescent nanoswitch control. J. Hazard. Mater. 429, 128316.
Xu, J., Yu, H., Hu, Y., Chen, M., Shao, S., 2016. A gold nanoparticle-based fluorescence sensor for high sensitive and selective detection of thiols in living cells. Biosens. Bioelectron. 75, 1–7.
Yang, J., Li, Z., Jia, Q., 2019. Design of dual-emission fluorescence sensor based on Cu nanoclusters with solvent-dependent effects: Visual detection of water via a smartphone. Sens. Actuators, B 297, 126807.
Yang, F., Lin, D., Pan, L., Zhu, J., Shen, J., Yang, L., Jiang, C., 2021. Portable Smartphone Platform Based on a Single Dual-Emissive Ratiometric Fluorescent Probe for Visual Detection of Isopropanol in Exhaled Breath. Anal. Chem. 93 (43), 14506–14513.
Yao, L., Zhou, F., Cai, M., Peng, Y., Sun, J., Chen, Q., Jin, X., Wang, G., Zhang, J., 2017. Development and validation of a sensitive LC-MS/MS method without derivatization/ion-pairing agents for etimicin quantification in rat plasma, internal ear and kidney. J. Pharm. Biomed. Anal. 146, 96–102.
Yin, Y., Chen, Z., Li, R.H., Yi, F., Liang, X.C., Cheng, S.Q., Wang, K., Sun, Y., Liu, Y., 2022. Highly Emissive Multipurpose Organoplatinum (II) Metallacycles with Contrasting Mechanoresponsive Features. Inorg Chem 61, 2883–2891.
Yuan, X., Bai, F., Ye, H., Zhao, H., Zhao, L., Xiong, Z., 2021. Smartphone-assisted ratiometric fluorescence sensing platform and logical device based on polydopamine nanoparticles and carbonized polymer dots for visual and point-of-care testing of glutathione. Anal. Chim. Acta 1188, 339165.
Yuan, Y.Z., Zhang, M., Fan, X.L., Wang, G.H., Hu, C.Q., Jin, S.H., Van Schepdael, A., Hoogmartens, J., Adams, E., 2012. Impurity profiling of etimicin sulfate by liquid chromatography ion-trap mass spectrometry. Journal of Chromatography B-analytical Technologies in the Biomedical and Life Sciences 70, 212–223.
Zha, J., Dong, C., Wang, X., Zhang, X., Xiao, X., Yang, X., 2017. Green synthesis and characterization of monodisperse gold nanoparticles using Ginkgo Biloba leaf extract. Optik 144, 511–521.
Zhuang, Y., Zhang, J., 2010. Electrochemiluminescence of an electrocatalytic action of etimicin on Tris(2,2'-bipyridyl) ruthenium (II) immobilized in Nafion modified carbon paste electrode. Luminescence 25 (4), 343–348.